Uplooking local resolution due to atmospheric turbulence

Amber L. Iler
KBR, Inc., 900 Victors Way Suite 220, Ann Arbor, MI 48108
Bobby R. Hunt and David G. Sheppard
KBR, Inc., 535 Lipoa Parkway, Suite 175, Kihei, HI USA 96753

ABSTRACT

Atmospheric turbulence is a major constraint on the ability of uplooking optical systems to gather information (including imagery) of objects orbiting the Earth. Better observations, for space domain and space situational awareness, depend on mitigating the effects of this turbulence.

An emerging, and fruitful, method in signal processing, Compressive Sensing (CS) through sparse and redundant representations, has been applied in recent years to atmospheric turbulence in optical uplooking telescopes [1, 2]. These new methods adopt alternative concepts for the representation of data in terms of a set of basis functions. Conventional tools of signal and image processing focus on Fourier series and transforms to generate representations of data. Conversely, CS creates basis sets of functions that do not possess the usual properties of orthonormality and minimality. CS compiles these basis sets from actual data and contains them in a collection of functions called a dictionary [3]. These dictionary methods have led to improvements in the mitigation of turbulence by the methods of blind deconvolution [2, 4]. However, the success of these dictionary methods relies on knowledge and access to dictionaries that encompass the turbulence present in observations.

Additionally, a continuing problem in atmospheric turbulence is anisoplanatism, where the point-spread-function (PSF) of the optical system varies with position across the image focal plane. In this situation, mitigation deblurring actions for one position must be adapted to different actions in a different focal plane position. Further, because a PSF determines resolution in an image region, anisoplanatism alters inherent resolution in different image positions. This was graphically pointed out by Fried in his classic paper on the probability of a diffraction-limited "Lucky Image" observed through turbulence [5]:

> *"It is appropriate to note that the probability we have calculated applies independently to separate isoplanatic patches on the image. This means that in any one image, rather than its being entirely good or entirely poor resolution, there will be distributed over the image field-of-view a set of rather small regions, isoplanatic patches, in which the resolution is good. The rest of the image area will have much poorer resolution."*

Fried's comments prompt an important question: What do the statistics of the resolutions, present in observations through turbulence, predict? The answer to this question is critical to planning and having available the necessary variety of dictionaries to be used in advanced blind deconvolution algorithms [4].

The analysis of Fried, deriving the probability of diffraction-limited imaging in turbulence, has a logical complement mandated by the laws of probability, i.e., the probability of "Unlucky Imaging". This is the probability that, in each anisoplanatic patch as described by Fried, there will be *less than* diffraction-limited resolution. From this viewpoint we show that:

- The Unlucky Image probability can be computed in simple numerical fashion from the calculated form of Lucky Image probability in Fried's analysis.
- The definitions of probability mean the Unlucky Image statistics describe a Cumulative Distribution Function (CDF).
- The CDF of the Unlucky Image can be converted into the corresponding Probability Density Function (PDF) of different resolutions in turbulent images.
- A PDF, so derived, gives the distribution of local resolution variability for Fried's descriptions of the Lucky Image behavior (quoted above), and the resolutions are directly related to the turbulence, parameterized by the Fried parameter, r_0, and the pupil diameter used in image formation.

We conclude by presenting a PDF of resolutions, computed from real PSFs experimentally collected in atmospheric turbulence, displaying the same shape and behavior as predicted by our "Unlucky Image" analysis. We disclose, further, another set of numerical observations, reported in the literature, that have the same behavior for the case of uplooking observations, as well as similar results for additional uplooking calculations beyond those referenced from the literature. Thus, we verify, for planning resources when imaging in turbulence, it is possible to estimate, from optical system properties and turbulence strength, the resolution variations expected in space-variant blind deconvolution of anisoplanatic behavior. This has immediate and direct application to the planning of resources and systems for collection of data for Space Domain Awareness (SDA). From these estimates, it is then possible to determine the range of dictionary resolution behaviors, which must be provided for dictionary-based turbulence mitigation to achieve adaptive blind deconvolution of observations for SDA.

1. INTRODUCTION

This paper was motivated by our previous research into the Compressive Sensing (CS) method of sparse and redundant dictionaries for representing atmospheric turbulence [1, 2, 6]. While conventional signal and image processing focuses on Fourier series and transforms to represent data, this CS method uses the K-means Singular Value Decomposition (K-SVD) algorithm to compile basis sets from actual data and contain them in a collection of functions called a dictionary [3]. This alternative approach represents data in terms of functions that are not orthonormal. While non-orthogonality may seem to be a disadvantage, the atoms in the derived basis set are better matched to the shapes to be represented, allowing them to be represented with a fewer bases. Application of these dictionary methods to optical point-spread-functions (PSFs) have led to improvements in the mitigation of turbulence by the methods of blind deconvolution [2, 4].

The concept of "local resolution" emerged when we applied sparse and redundant PSF dictionaries to the problem of block-based MultiFrame Blind Decovolution (MFBD). While block-based approaches for processing space-variant imagery have been generally accepted by the signal and image processing community since the 1990s [7], the theory motivating this approach was derived from anisoplanatic characteristics in the pupil plane, where the extent of turbulent PSF variation is understood as a function of isoplanatic angle, illustrated in Fig. 1. We sought to understand how anisoplanatism affects resolution statistics in the *focal plane* and the implications this might have for MFBD image restoration.

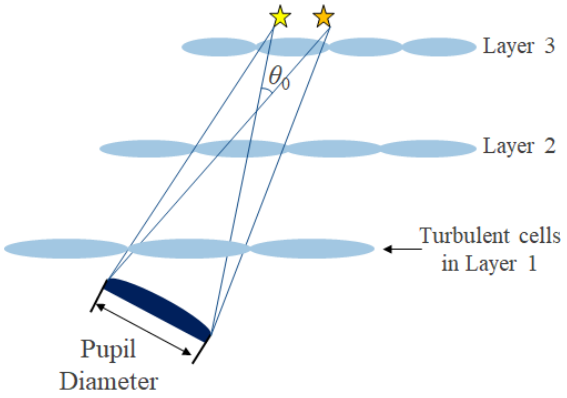

Fig. 1: The pupil plane angle over which the column of turbulence is the same for two objects defines the isoplanatic angle, θ_0.

To do this, we returned to Fried's "Lucky Image" paper, where he describes the statistical behavior of isoplanatic patches [5], as quoted above in the Abstract. We postulated that isoplanatic patch statistics can be used to inform the number and variety of dictionaries needed to support MFBD image restoration by understanding how the statistics translate to the image plane. This was demonstrated by deriving the "Unlucky Image" probability distribution, then using the derived Unlucky Image statistics to define a Cumulative Distribution Function (CDF). The derivative of the CDF then provides the corresponding Probability Density Function (PDF) of different resolutions across the image plane. This PDF provides insight into the variability of resolution that can be expected in the image plane as a function of the Fried parameter, r_0, and the pupil diameter, D, used in image formation. In this way, pupil plane isoplanatic behavior provides insight into focal plane characteristics, which we referred to as local resolution statistics [8]. These concepts were tested using downlooking point source data and the findings supported application of local resolution statistics for informing selection of MFBD image restoration parameters [8]. Furthermore, our downlooking findings were supported by another set of numerical observations, reported in the literature, that had the same behavior for uplooking observations [9].

In this paper, we will verify the same trends seen in Refs. [8] and [9] apply to a simulated uplooking Space Domain Awareness (SDA) scenario. We provide simulation details and present several different PDFs for ensquared regions in the image plane, showing it is possible to estimate, from optical system properties and turbulence strength, the

resolution variations expected in SDA applications. This has immediate and direct application to the planning of resources and systems for SDA by enabling determination of dictionary resolution behaviors and choice of block sizes for use in MFBD.

2. APPROACH

Because PSFs acquired through turbulence show a great variety in distribution and gross morphological characteristics, we sought to simulate data covering the areas of highest interest in terms of D/r_0. We generated PSFs for five D/r_0 levels for a hypothetical Raven-class telescope located in Kihei, HI and imaging the International Space Station (ISS). The telescope optics were defined to have D = 0.406 m and $f/\#$ = 6.03. For the focal plane optics, we simulated a Canon PowerShot G7 camera with pixel pitch of 2 µm, resulting in a nearly Nyquist-sampled quality factor, Q = 1.8. Our simulated wavelength was defined as the center of the V-band at 551 nm. We located the ISS in our simulation at an altitude of 400 km and a zenith angle of 10° to the telescope. Atmospheric turbulence was simulated using the wavefront propagation method of [10] for 1000 128x128 PSFs through 10 turbulent layers using the Huffnagel-Valley 5/7 C_n^2 model at five incremental levels of r_o: [0.1366, 0.1021, 0.0840, 0.0725, 0.0644] m.

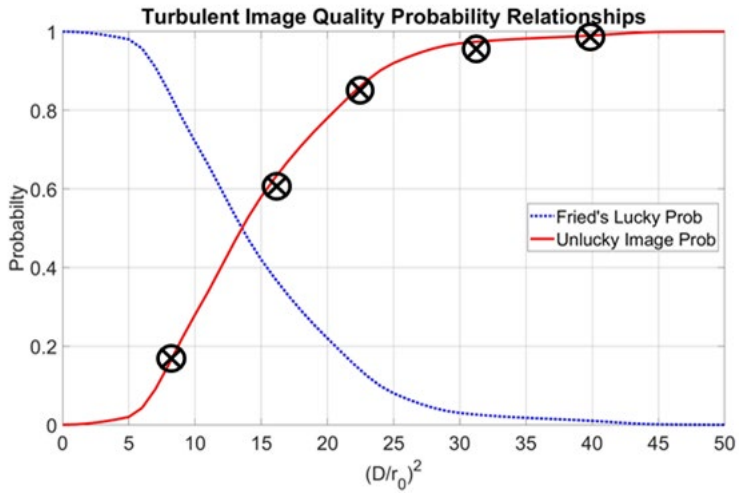

Fig. 2: Our five simulated SDA turbulence levels cover Unlucky Image regimes from rarely Unlucky to always Unlucky.

Fig. 2 illustrates the turbulence regimes that resulted, in terms of Fried's Lucky Image probability and the corresponding Unlucky Image probability, as reported in [8]. At the first $\left(\frac{D}{r_o}\right)^2$ level of 8.84, we see the PSFs should, for the most part, be in the Lucky Imaging, or mild turbulence, regime, with less than 20% of them being Unlucky. The second level, corresponding to $\left(\frac{D}{r_o}\right)^2 = 15.83$ will be Unlucky about 60% of the time, and so on. The final value of 39.74 is very near the upper asymptote of the Unlucky Image probability, suggesting all PSFs for this case will be Unlucky.

Through fixing the diameter, D, in our simulations, we expect the local resolutions of Fried's isoplanatic patches will vary as though there are many different optical apertures applying to each patch, according to r_o. Thus, because of the Fourier equivalence of point sources in the focal plane with PSFs in the pupil plane, we can expect the effective pupil diameter resulting from the five levels of r_o will vary according to the probabilities seen in the PDF of Fig. 3.

Fig. 3 illustrates how our simulated PSFs cover the full range of turbulent probability distributions, providing further insight into the statistical behavior predicted for these five regimes. At the first three $\left(\frac{D}{r_o}\right)^2$ levels, the PDF predicts the most variability in PSF characteristics, having some PSFs that are Lucky (i.e., compact) and others that are Unlucky (i.e, "splattered"), in varying amounts. For the final $\left(\frac{D}{r_o}\right)^2$ level, we expect variability will be considerably smaller, because, as mentioned above, we expect nearly all PSFs for this case to be Unlucky.

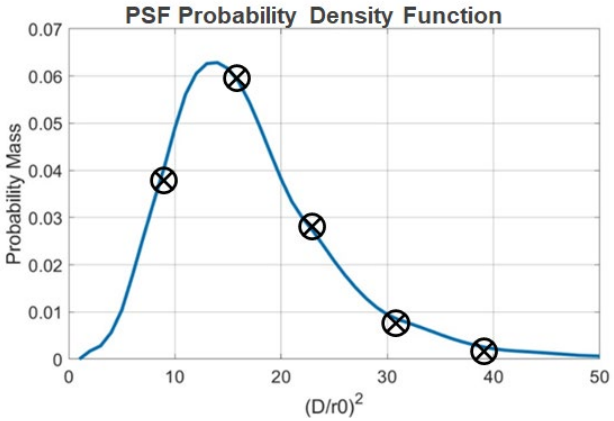

Fig. 3: The five simulated levels cover both high PSF variability (at left) and low variability turbulence regimes (right).

To better understand how these hypothetical SDA turbulence scenarios relate to the variety of dictionaries and focal plane block-sizes for use in MFBD, we chose the

same metric of ensquarement as was used in [8]. Ensquarement calculates the mass distribution within a square region of focal plane pixels. Because this value is calculated in the focal plane, it allows us to directly relate ensquarement statistics to predicted local resolution behavior.

To calculate ensquarement, we adjusted the center-of-mass of each simulated point source (equivalent to the PSF in the pupil plane) to be centered within a square of the size chosen. It is worth noting that this process effectively mimics a local tip/tilt correction process, to slightly shift the PSF. We then computed the fraction of the PSF energy that fell within the square. For a diffraction limited PSF, we would expect a square with width the size of the Airy disk would contain the majority of a PSF mass. In our previous work, we found this diffraction limited condition was reached when 95% of the PSF energy was ensquared [8]. Thus, to gain a better understanding of local resolution, we focused on two different ensquarement sizes: 33x33 and 15x15 pixel^2 areas of the focal plane.

3. RESULTS

For our 33x33 ensquarement regions, we average ensquarement fractions of [0.9702, 0.9614, 0.9522, 0.9426, 0.9311] were calculated for the 1000 PSFs at each turbulence level. To better illustrate the relationship of ensquarement levels with PSF energy, we display a randomly selected PSF from the most severe turbulence case in Fig. 4, along with a 33x33 pixel^2 box overlaid in white. As can be seen in this exaggerated display, low amounts of PSF energy are simulated across the full extent of the 128x128 pixel^2 region. However, when the centermost 33x33 region is displayed in a standard minimum-to-maximum range stretch (inset, Fig. 4), we see that the majority of the PSF energy is apparent within this region. As discussed in [8], the 95% ensquarement level, just missed in the case of the PSF in Fig. 4, captures the majority of the PSF contained within the first dark ring of the Airy disc. Hence, one might expect image restoration through blind deconvolution for a region of this size should have sufficient PSF energy available to reach diffraction limited resolution, if Lucky conditions should occur.

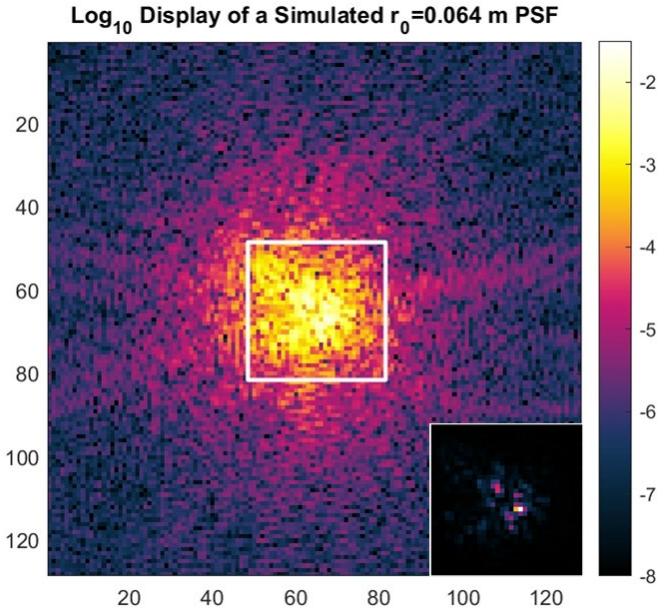

Fig. 4: Logarithmic display of a simulated PSF at the strongest turbulence level with a 33x33 pixel^2 box overlaid. Inset shows the inner 33x33 region displayed with a standard min/max stretch.

We also note here that, without the slight shift due to the tip/tilt correction step described above, the fractional ensquarement values for this size box would be smaller than stated above and a larger box would be needed to reach the same ensquarement fraction levels. Though with nearly 95% ensquarement for all five regimes, we expect the 33x33 calculations provide insight into optimal cases of local resolution variability for image plane regions of this size.

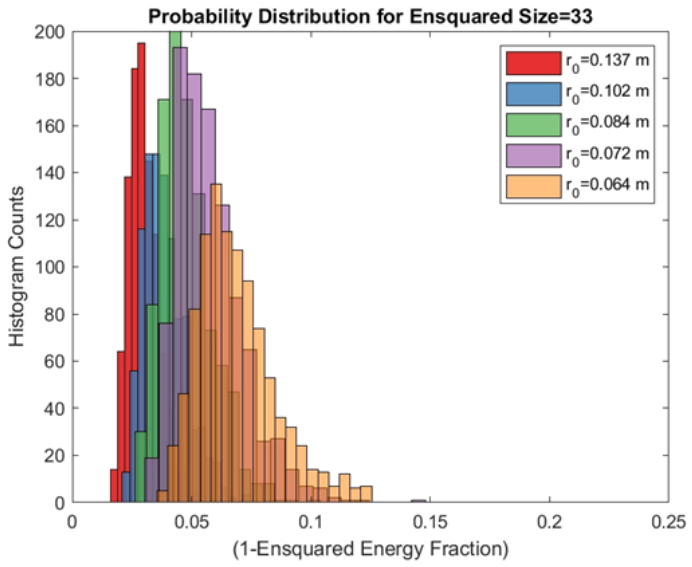

Fig. 5: Probability that a 33x33 image plane region will not produce diffraction limited resolution when a Lucky Image occurs for the five r_0 levels of our SDA simulation.

Fig. 5 shows overlapping, partially transparent histograms for the 33x33 ensquarement fractions at the five turbulence levels in our SDA simulation. We have plotted these as 1-ensquarement to liken them to the Unlucky Image PDF shape, shown in Fig. 3. All five of the histograms match this shape. We also see that, as the amount of turbulence increases (i.e., r_o decreases), the "Unluckiness" of the distributions increase, indicated by the distribution shifts to the right. The reduction in ensquarement as one moves to the right, of course, indicates that the corresponding PSFs are broadening or becoming more irregular. We interpret this as a change in likelihood that blind deconvolution of a 33x33 region of the focal plane will result in a diffraction limited result when a Lucky Image occurs.

We also see the Fig. 5 histograms widen as r_o worsens. This is not unexpected, because the lower average ensquarement of less than 95% for the final two levels indicates that less diffraction limited energy from the more splattered PSFs will be captured within a 33x33 region. As such, we note the widths of the five histograms are not a fair way to compare the overall PSF variability at each level. For a fair comparison, we would need to plot histograms with identical ensquarement fractions, which would likely require five different ensquarement sizes.

Next, we turn to the 15x15 ensquarements. For this size, we calculated average ensquarement fractions of [0.9002, 0.8544, 0.8090, 0.7593, 0.7114] for the 1000 PSFs at each turbulence level, indicating all cases will be less likely to achieve diffraction limited resolution when a Lucky Image occurs. Correspondingly, the histograms displayed in Fig. 6 are shifted significantly along the x-axis (note the overall change in x-axis scale), in comparison to those in Fig. 5. This shift indicates an increase in "Unluckiness" for 15x15 pixel^2 regions of the focal plane, which we interpret as an increase in likelihood that blind deconvolution will not be able to produce diffraction limited resolution when a Lucky Image occurs.

As with the 33x33 ensquarements, we see that the 15x15 histograms in Fig. 6 widen in distribution as the turbulence worsens. This widening occurs because the amount of PSF energy that falls outside of the 15x15 ensquared regions is increasing as the PSFs become more splattered, as indicated by the decreasing average ensquarement factions. However, we note that, even though a significant portion of PSF energy is missed for the final two turbulence levels, all five of the histograms match the expected PDF shape predicted by Fried's analysis, and shown in Fig. 3 above.

These results can be further understood through visual inspection of the PSFs at the different ensquarement sizes. Randomly selected PSFs from our

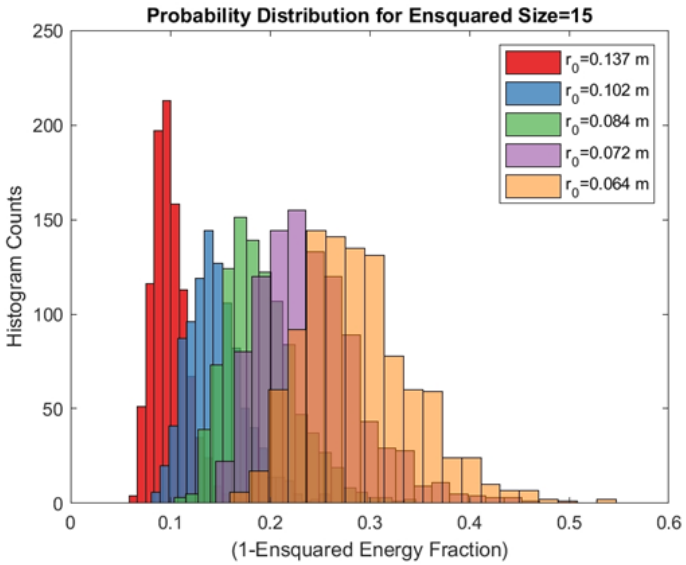

Fig. 6: Increasing likelihood, as a fumction of r_0, that diffraction limited resolution will not be achieved for an image plane region of 15x15 pixels^2.

simulation were ensquared, as described above, and displayed side-by-side in Fig. 7 for a 33x33 array size (top row) and 15x15 arrays (bottom). First, we note that the value of r_o decreases from left to right. Despite this, for this randomly selected example, we see that the PSF for the second turbulence level appears more concentrated than the PSF at the lowest turbulence level (shown in the first column). This coincidence is representative of the near-Lucky circumstance for the second set, relative to all the other cases.

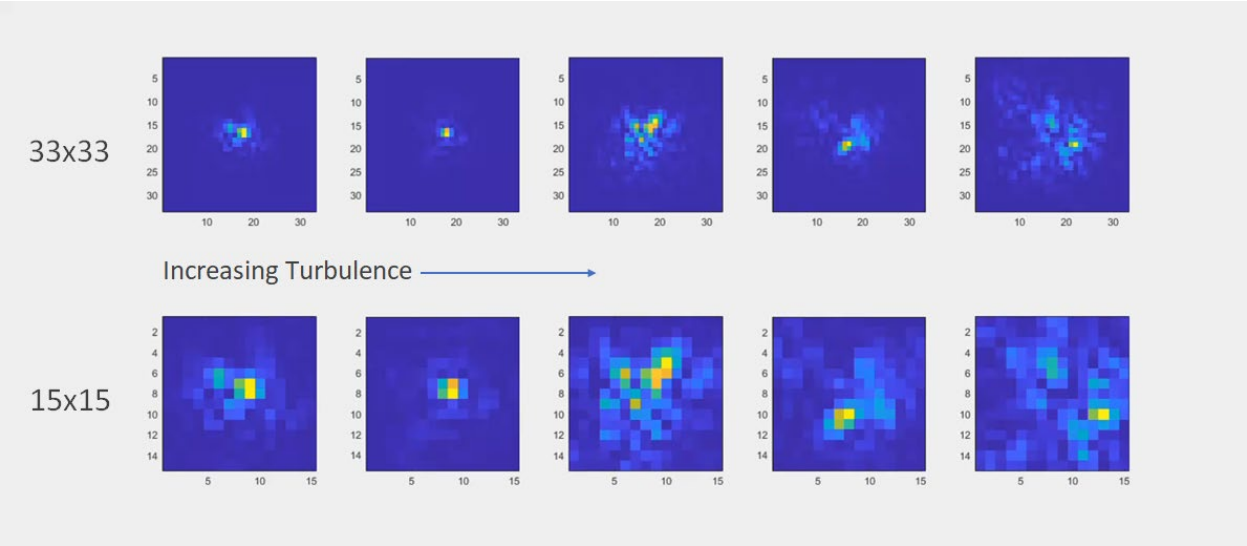

Fig. 7: Illustration of PSF energy ensquared at the two different ensquarement levels for the five turbulence levels (increasing turbulence shown from left to right. Top row shows 33x33 ensquarements, bottom row shows 15x15 ensquarements.

Because the five PSFs displayed in the first row of Fig. 7 are the same as those in the second row, it is easy to visually see how a large amount of the PSF energy is missed for the final r_o level at the 15x15 ensquarement. In fact, because center-of-mass was used to center each PSF relative to the ensquared area, rather than the peak value location, the PSF peak for that case ends up only two pixels from the edge of the ensquared area. In this particular PSF, one can easily visualize that blind deconvolution of a 12x12 block from this area of the image would miss so much of the PSF energy that it would be virtually impossible to achieve diffraction limited resolution for a focal plane patch of this size.

4. CONCLUSIONS

We conclude by presenting, in Fig. 8, the PDF of local resolutions computed from real PSFs experimentally collected under a downlooking scenario in the presence of anisoplanatic turbulence. In this figure we show the 35x35 focal plane ensquarement fractions calculated for these PSFs, as it originally appeared in [8]. Note how the shape of this distribution matches the same narrow peak at the left and long tail to the right form seen in our simulated uplooking PSFs ensquared in Fig. 6 and Fig. 7. In addition, other teams have previously used similar metrics, in one case Strehl ratio [9] and another case ensquarement [11], to examine the variability of anisoplanatic turbulence with similarly shaped results.

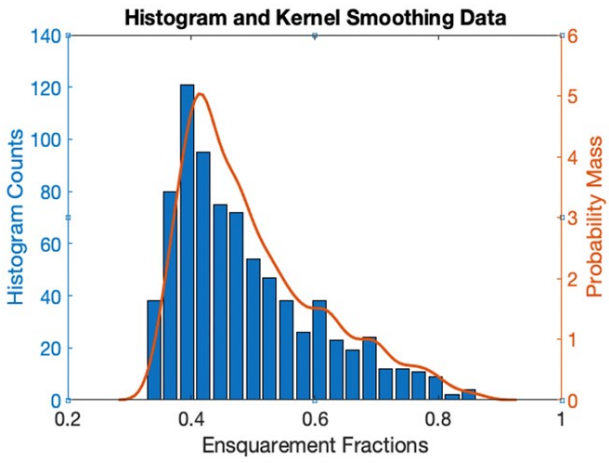

Fig. 8: Histogram of the 35x35 ensquarement energy fractions for real PSF data, as originally published in [8].

Thus, we conclude our simulated SDA scenario verifies how local resolution statistics can be used for planning resources when imaging in turbulence, given knowledge of D/r_0. We assert the consistency of our

simulated ensquarement results with Fried's Lucky Image probability relationship shows that it is possible to estimate, simply from optical system properties and turbulence strength, the resolution variations expected for space-variant blind deconvolution of anisoplanatic turbulence. The PSF probability density relationship calculated from ensquared PSFs provides this insight through histogram binning of the metrics. This approach is valid because these results relate directly to how much PSF energy is available within a corresponding region of the focal plane. Correspondingly, this relates to the likelihood of getting a "good" PSF deconvolution using block-based, spatially-variant turbulence mitigation techniques. In other words, the block size for such block-based deconvolutions should be consistent with ensquarement, since a PSF in a deconvolution solution with a block that is too small will not possess all significant structure. Conversely, a block that is too large will mix adjoining PSFs. Thus, two sizes must be considered: The size of the PSF for that area of the image and the distance over which the local PSF is approximately constant. Choosing block sizes that capture most PSF structure, as related to the ensquarement statistics in Fig. 6, Fig. 7, and Fig. 8, will achieve the best "Goldilocks" result (i.e., "…just right").

This has immediate and direct application to the planning of resources and systems for collection of data for SDA. For example, from these estimates, it is then possible to determine the range of CS dictionary resolution behaviors, which must be provided for dictionary-based turbulence mitigation to achieve adaptive blind deconvolution of observations for SDA. Additionally, exploitation of local resolution relationships could be used to optimize optical system design by examining expected values of D/r_0 and using the PDF relationship to choose different aperture size or f-stop for expected system turbulence conditions. The same analyses could also lead to identification of situations when adaptive optics might be most beneficial or more likely to achieve diffraction limited resolution. We recommend verification of the trends shown here through experimental collection of anisoplanatic point source data for optical systems of highest interest to the SDA community.

5. REFERENCES

[1] B. R. Hunt and K. Knox, "Sparse and Redundant Dictionaries in Representation of Atmospheric Turbulence Point Spread Functions," in *OSA Classical Optics Congress*, Big Island, HI, 2014.

[2] B. R. Hunt and K. Knox, "Optimal Dictionaries for Sparse Solutions of Multi-Frame Blind Deconvolution," in *AMOS Conference Proceedings*, Maui, HI, 2014.

[3] M. Elad, Sparse and Redundant Representations, New York: Springer-Verlag, 2010.

[4] D. G. Sheppard, B. R. Hunt and A. L. Iler, "Block-based streaming blind deconvolution for space-variant turbulence mitigation," in *Proc. SPIE 11836, Unconventional Imaging and Adaptive Optics 2021*, San Diego, CA, 2021.

[5] D. L. Fried, "Probability of getting a lucky short exposure image through turbulence," *J. Opt. Soc. Am. A.,* vol. 68, no. 12, pp. 1651-1658, 1978.

[6] B. Hunt, A. L. Iler, C. A. Bailey and M. A. Rucci, "Synthesis of Atmospheric Turbulence PSFs by Sparse and Redundant Representations," *Optical Engineering,* vol. 57, no. 2, p. 024101, 2018.

[7] T. E. Bishop, S. D. Babacan, B. Amizic, A. K. Katsaggelos, T. Chan and R. Molina, "Blind Image Deconvolution: Problem formulation and existing approaches," in *Blind image deconvolution: theory and applications*, Boca Raton, CRC Press, 2001, pp. 1-41.

[8] B. R. Hunt, A. L. Iler and D. G. Sheppard, "Local resolution characteristics of atmospheric turbulence," *Optics Express,* vol. 30, no. 9, p. #457417, 2022.

[9] N. M. Law, C. D. MacKay, R. G. Dekany, M. Ireland, J. P. Lloyd, A. M. Moore, J. G. Robertson, P. Tuthill and H. C. Woodruff, "Getting lucky with adaptive optics: Fast adaptive optics image selection in the visible with a large telescope," *ApJ,* vol. 692, no. 1, pp. 924-930, 2009.

[10] M. C. Roggemann and B. M. Welsh, Imaging Through Turbulence, Boca Raton, FL: CRC Press, 1996.

[11] T. J. Rogne and et al., "Experimental evidence for spatial stabilization of deep-turbulence-induced anisoplanatic blur," *Optics Express,* vol. 27, no. 23, p. 32938, 2019.